Renewable Energy 219 (2023) 119473

Contents lists available at ScienceDirect

Renewable Energy

journal homepage: www.elsevier.com/locate/renene

Comparing methods for the long-term performance assessment of bifacial photovoltaic modules in Nordic conditions

Lauri Karttunen [a,*], Sami Jouttijärvi [a], Aapo Poskela [a], Heikki Palonen [a], Hugo Huerta [b], Milica Todorović [a], Samuli Ranta [b], Kati Miettunen [a]

[a] Department of Mechanical and Materials Engineering, Faculty of Technology, University of Turku, Vesilinnantie 5, 20500, Turku, Finland
[b] Department of Chemical Industry, Faculty of Engineering and Business, Turku University of Applied Sciences, Joukahaisenkatu 7, 20520, Turku, Finland

ARTICLE INFO

Keywords:
Performance loss rate
High latitudes
Photovoltaic performance
Bifacial photovoltaics
Performance metric

ABSTRACT

The main objective of this study is to discover which performance loss rate (PLR) calculation methods provide the most reliable results for vertical bifacial photovoltaics (VBPV) in Nordic conditions. For this purpose, over 1600 filter-metric-aggregation-model combinations for PLR calculation are compared. Accurate determination of PLR is crucial for estimating the economic profitability of a PV system, but standardized methodology is lacking as is the understanding on how the common PLR calculation frameworks perform for both VBPV technology and Nordic climatic region. Here, four-year, minute-resolution datasets from adjacent VBPV modules and a weather station in Turku, Finland (60°N) are used. After removing crude outliers, a benchmark PLR of -1.46 ± 0.03 %/year was obtained by averaging the remaining over 1200 filter-metric-aggregation-model combinations. The year-on-year method with a daily/weekly aggregated temperature- and irradiance-corrected performance model was found robust and reliable to Nordic high seasonality. In contrast, several commonly used methods, such as the PVUSA model, produced unrealistic results. Unexpectedly, temperature correction increased the seasonal pattern of the performance ratio, and PLR varied with irradiance conditions and between the front and rear sides of the module. This work expands the best practices of PLR calculation to complement the development of global PLR calculation standards.

1. Introduction

Solar energy is globally one of the fastest growing energy sources [1], and the accurate long-term performance assessment of solar photovoltaic (PV) systems is crucial to provide reliable lifetime predictions and to prevent financial risks [2]. Long-term performance can be characterized by measuring annual energy yields, performance metrics, degradation rates, and performance losses [3]. The degradation rates and performance losses can be assessed from IV curve measurements as the difference between the initial and recent values of electrical parameters [4–6], or using continuous performance data and applying statistical methods to this performance time series to obtain the loss rate [7–10]. This study focuses on the statistical evaluation of performance losses, including both permanent effects, such as module or system degradation, and reversible effects, such as soiling and snow coverage. Typically, long-term performance losses are expressed in the form of performance loss rate (PLR), which represents a system's linear loss in performance, usually given in a unit of %/year [11]. PLR is an important measure since it can be used to evaluate the current stage of a system's or module's performance as well as to obtain lifetime predictions, helping to assess economic profitability. Because PLR is often used to infer the long-term performance of the PV system, high-quality datasets collected over multiple years are the basis of reliable statistical PLR calculation. This study presents a novel four-year dataset of a vertical bifacial PV (VBPV) module with its ambient weather in Nordic conditions.

The lack of a standardized approach to calculate PLR is problematic since different methods have been reported to produce highly varying PLRs [12,13]. Various comparative studies have suggested best practices and elements for a standardized methodology. Some of them have focused on individual performance/PLR calculation steps, such as data quality analysis and pre-processing [14–16], performance modeling [17–19], statistical methods and time-series feature correction for PLR assessment [9,20–23], whereas some of them compare the different approaches as a whole, covering all calculation steps [11,12,24,25]. One of the recent efforts to study PLR calculation was a part of the International Energy Agency's Photovoltaic Power Systems Programme (IEA's PVPS) Task 13 [26]. As a part of this task, an international study by

* Corresponding author.
E-mail address: lauri.p.karttunen@utu.fi (L. Karttunen).

https://doi.org/10.1016/j.renene.2023.119473
Received 28 April 2023; Received in revised form 18 September 2023; Accepted 15 October 2023
Available online 16 October 2023

Nomenclature

AM1.5	Reference spectrum, corresponding to 1.5 atm thickness
BF	Bifaciality factor
C	Temperature correction term
CS	Clear-sky
c-Si	Crystalline silicon
CSI	Clear-sky index
EM3	Dataset including electrical data from the solar module
$G_{E,BPV}$	Effective bifacial POA irradiance (W/m^2)
G_{front}	POA irradiance incident on the front side (W/m^2)
G_{rear}	POA irradiance incident on the rear side (W/m^2)
G_{ref}	Reference POA irradiance (1000 W/m^2)
I	Output current (A)
LL/POA LL	Irradiance lower limit
P	Power (W)
P_0	Rated power of the module (W)
PI	Performance index
PLR	Performance loss rate (%/year)
$\overline{PLR}$	Estimated real system PLR
PR	Performance ratio
PRt	Temperature-corrected performance ratio
PVUSA	Rating method developed in PVUSA project
RCTC	Dataset including reference cell and thermocouple data
T_{air}	Air temperature (°C)
T_c	Cell temperature (°C)
T_m	Module (front) surface temperature (°C)
T_{ref}	Reference temperature (25 °C)
V	Output voltage (V)
WS	Wind speed (m/s)
Y_f	Final yield of a PV system (kWh)
Y_r	Reference yield of a PV system (kWh)
6k	Regression model with 6 fitting parameters
ΔT	Temperature difference between module surface and cells (°C)

Abbreviations

AC	Alternating current
BPV	Bifacial photovoltaics
BSTC	Bifacial standard test conditions
DC	Direct current
EM	Energy meter
GHI	Global horizontal irradiance (W/m^2)
IEC	International Electrotechnical Commission
IV	Current-voltage
LSLR	Least squares linear regression
MPP	Maximum power point
OC	Open circuit
POA	Plane-of-array (W/m^2)
RC	Reference cell
RLR	Robust linear regression
SC	Short circuit
SD	Standard deviation
STC	Standard test conditions
TC	Thermocouple
VBPV	Vertically mounted BPV
YOY	Year-on-year method

Greek letters

α	Temperature coefficient of current (%/°C)
τ	Duration of recording interval (s)
γ	Temperature coefficient of power (%/°C)

Lindig et al. [11] was conducted to develop a framework for PLR calculation and benchmark different calculation approaches across various climatic zones. Based on this work and the other studies in the field, Lindig et al. also compiled the best practices for PV PLR calculations [24]. In addition to the numerous studies, various open-source tools for performance analysis and PLR calculation have been developed, such as RdTools for Python [27] and PVplr for R [28,29], to reduce the possible variability of PLR values by providing a set of ready-to-use methods. Based on the current practices, the statistical PLR calculation pipeline can be divided into the following steps: (a) initial data quality assessment, (b) data filtering, (c) performance metric calculation and data aggregation, (d) possible performance time-series feature corrections, and (e) the calculation of the actual PLR using a statistical model [24]. Although the general pipeline from step (a) to (e) is well established, the choice of methods for each step can dramatically affect the results. In this study, various methods for each calculation step are considered and carefully analyzed, resulting over 1600 filter-metric-aggregation-model combinations to calculate the PLR, thus contributing to global efforts to develop standardized and reliable PLR calculation frameworks.

Besides the lack of standards, significant literature gaps considering certain technologies, especially bifacial PV (BPV), and geographical areas exist for PLR calculations. Some of the comparative PLR calculation studies, such as [7,26,30,31], have been a part of large international and inter-laboratory projects, comparing methods by using data from many PV sites across different climatic conditions. However, none of the data used in these studies are from Nordic conditions. Altogether, there are only few case studies on the long-term performance and PLR calculation in Nordic areas, which mainly compare performance under standard test conditions (STC) using few datapoints across multiple years to obtain performance losses [5,6]. Paudyal and Imenes [32] studied the long-term performance more extensively using different data aggregation intervals and investigating the effect of spectral correction (commonly excluded) with performance time-series data. Øgaard et al. [33] compared different data filtering approaches and performance metrics in Nordic conditions and concluded that tailored filters for effects that cause variability in performance metric data, such as snow, curtailment, and systematic irradiance difference over the system, increase the reliability of performance monitoring. Our recent work displayed that Nordic conditions induce large gaps in the performance time series data during winters and that various PLR methods result in greatly differing PLRs [34]. Regarding bifacial technology, Mannino et al. [35] studied the PLR of bifacial modules in the Southern Italy over two years by applying a 5-step PLR calculation workflow based on the best practices presented in Ref. [24]. They used three different variations of performance ratio (PR) with linear regression to obtain PLR, and compared the results to a solar simulator flash test. PLR was found to be high, around −1.8 %/year, and there were no large differences between PLRs of the three PR metrics. Our work presents a substantially greater number of different PLR calculation method combinations in a similar type of PLR study, applied for a differently oriented bifacial system at different location.

In general, the under-representation of Nordic conditions is common in the PV field, possibly due to the belief that the northern conditions make the Nordics unsuitable for PV installations [36]. Northern conditions are characterized by large seasonal variation in temperature, solar radiation, and daytime length as well as long, dark, and cold winters and warm summers with long days. However, solar irradiation in Finland is almost the same as in Germany [37,38]. Additionally, the lower ambient temperatures favor the power generation of silicon solar cells, which have higher efficiency in low temperatures. The green transition has been accelerated by the recent energy crisis, which has increased

interest in Nordic PV as well. Overall, there is a large unutilized potential for solar PV in the Nordic countries and an urgency to harvest it. Thus, the analysis of the PLR of a VBPV system in Nordic conditions presented here is highly timely.

Bifacial modules, which can absorb light from both sides, can be installed conventionally, pointing towards the Equator, which allows the rear sides of the modules to absorb light reflected from the ground. East-west-oriented VBPV can be used to alter the production profile so that there are two production peaks: one in the morning and one in the afternoon. Such a production profile matches better with the consumption profiles of typical households and typical electricity peak prices, and thus a vertical east-west BPV system can achieve higher self-consumption rates compared to a conventional south-facing system [39, 40]. Furthermore, the overall production of east-west mounted VBPV can reach a higher overall production in the Nordics, where the solar elevation angle is low [41]. Due to good matching with peak prices and high overall production, VBPV is interesting for investment purposes as well.

Since the research areas of long-term performance and PLR assessment are currently vigorous, comprehensive research on performance assessment both in northern climates and for bifacial technology is needed to fill these corresponding literature gaps. This is especially important since high latitudes create difficulties in performance analysis, such as the following: (1) Highly varying weather conditions create strong seasonal patterns in performance time-series data, which impedes the accuracy of PLR estimation [7]. (2) Cold temperatures and low irradiance especially during winters create conditions far from STC, under which the PLR can vary compared to PLR obtained under STC [11]. (3) The current performance models are largely valid only under STC. The lack of insight proceeds directly from a lack of datasets and information on the output of BPV technology installed in northern regions.

This work addresses this literature gap by reporting a comprehensive analysis of over 1600 different PLR calculation method combinations, applied to determine the PLR of a VBPV module in Turku, Finland (60°N). The main objectives are to discover (a) which PLR calculation methods provide the most reliable results in the context of VBPV in Nordic conditions and (b) which common data filters and performance metrics are suitable for this type of data. The methods of this work were chosen largely based on the international benchmark study by Lindig et al. [11] and they are presented in Fig. 1 with a PLR calculation workflow. The analysis is carried out with a unique minute-level dataset, compiled from measurements from a test site consisting of VBPV modules equipped with power, temperature, and plane-of-array (POA) irradiance sensors, together with an adjacent weather station with temperature, wind speed and global horizontal irradiance (GHI) sensors. The long duration and high resolution of the used dataset, combined with a comprehensive comparative analysis and rarely studied PV technology and geographic area, provides unique insights on PLR calculation in these conditions. This understanding of the best PLR calculation methods promotes the adaptation of PV as a clean electricity source in Nordics and complements the development of global PLR calculation standards.

The structure of this work is as follows. Experimental setup and methods for performance analysis are described in section 2. Section 3 presents results and discussion about data quality, the effects of various data processing steps, the estimation of the real PLR of the module, the irradiance-dependency of PLR, and the comparison of the different PLR calculation approaches. Section 4 concludes the key results and discusses their implications.

2. Methodology

2.1. Experimental setups and data collection

The monitored field system consists of four vertically mounted (front

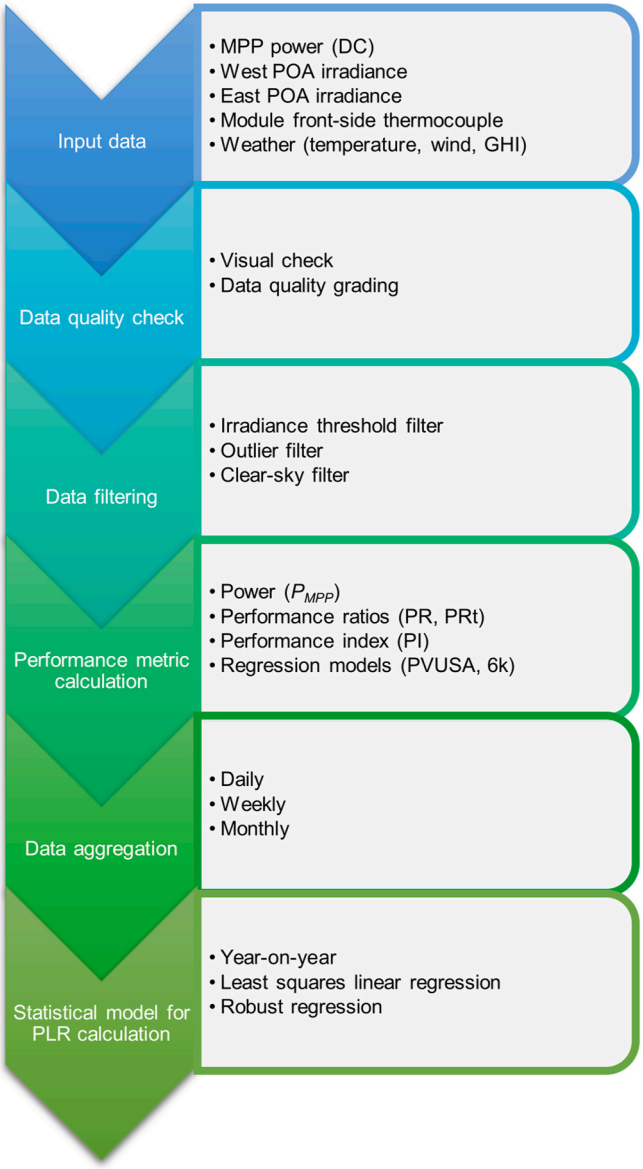

Fig. 1. PLR calculation workflow and different methods used in this work.

side facing east) frameless glass-glass bifacial modules (Prism Solar model Bi60-375BSTC [42]), installed on the rooftop of Turku University of Applied Sciences (TUAS) in Turku, Southwestern Finland (60°N, 22°E) in 2017. Each module has a DC-DC optimizer to keep the module at maximum power point (MPP), a DC energy meter (EM) to measure the DC current and voltage, and a T-type thermocouple (TC) attached to the front side to measure module surface temperature. In this study, data from one module (Module 3) located in the middle of the module array is considered. The POA irradiance is monitored by two reference cells (RCs) at the top of the modules, one facing east and the other facing west. The setup is shown in Fig. 2. A weather station with wind, temperature, and humidity sensors, and two secondary standard/class A [43] pyranometers for GHI measurements is in near proximity to the field test setup. A schematic diagram of the system setup (excluding the separate weather station) is presented in Fig. 3. The GHI pyranometers were cleaned regularly to prevent soiling errors but no cleaning was done for the vertical modules or RCs since there is no evidence of soiling, and generally vertically oriented modules show little to no soiling [44]. The electrical parameters (provided by the manufacturer) of the module are presented in Table 1. Parameters are presented separately for front

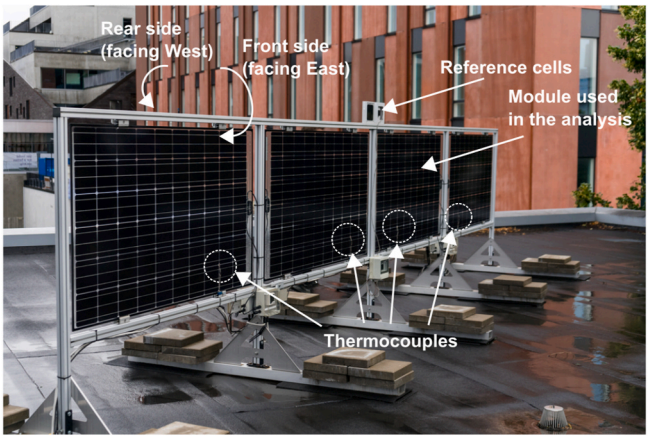

Fig. 2. Outdoor test setup of TUAS with four bifacial modules, two reference cells, and thermocouples to monitor module surface temperature. In this study, one of the modules is analyzed. Modified from photograph by Nyberg/UTU.

and rear side at STC, and for bifacial test conditions (BSTC, cell temp. 25 °C, AM1.5, 1000 W/m^2 (front) + 300 W/m^2 (rear)), defined by the manufacturer.

Different data sources are logged and stored separately: (1) the module has its own EM, (2) POA irradiances and TC readings are logged with an analog data acquisition module, and (3) weather station data are monitored with a weather transmitter with its own data logger. Therefore, three separate datasets were obtained, here referred to as EM 3 (EM3), RC and TC (RCTC), and weather data, respectively. EM3 and RCTC data collection started after system installation in August 2017, whereas weather data collection started in January 2018. In this study, data from August 2017 to July 2021 are used. The pyranometers were removed to another location in September 2020, which resulted in a lack of GHI measurement during the last 10 months of data. All data are logged with 1-min resolution. All monitored variables with corresponding start and end dates are presented in Table 2. All datasets used in this study have been made available to the research community [45].

2.2. Weather profile in Nordic conditions

The data is from high latitude (60°N, 22°E) conditions, which are characterized by strong seasonal weather patterns with cold and dark winter periods. To illustrate these conditions, GHI, air temperature, and wind speed data from the weather station are presented in Fig. 4 and Table 3. Raw minute-level data over the whole measuring period are considered, excluding nighttime data (nighttime filter is described in section 2.4). In Fig. 4A, the monthly means of GHI and air temperatures illustrate the seasonal cycle: during the summer months, irradiance and temperature reach their peak, whereas the winter months have sub-zero temperatures and very low irradiance. In Fig. 4B, the wind speed histogram showcases that most of the time wind speed is below 3 m/s, and rarely exceeds 5 m/s. In Table 3, the mean, minimum, and maximum values are presented for these three weather variables for each monitoring year, considering again only daytime data. Additionally, the

Table 1
Manufacturer's specifications for the module.

Electrical parameter	Front STC	Rear STC	BSTC[a]
Rated power (W)	295	266	375
DC voltage at MPP (V)	32.4	32.4	32.4
DC current at MPP (A)	9.10	8.19	11.6
Module efficiency (%)	17.7	15.9	22.5
Power temperature coefficient (%/°C)	−0.4139		
Current temperature coefficient (%/°C)	+0.0413		

[a] Bifacial STC (BSTC) = cell temp 25 °C, AM1.5, 1,000W/m^2 (front) + 300W/m^2 (rear).

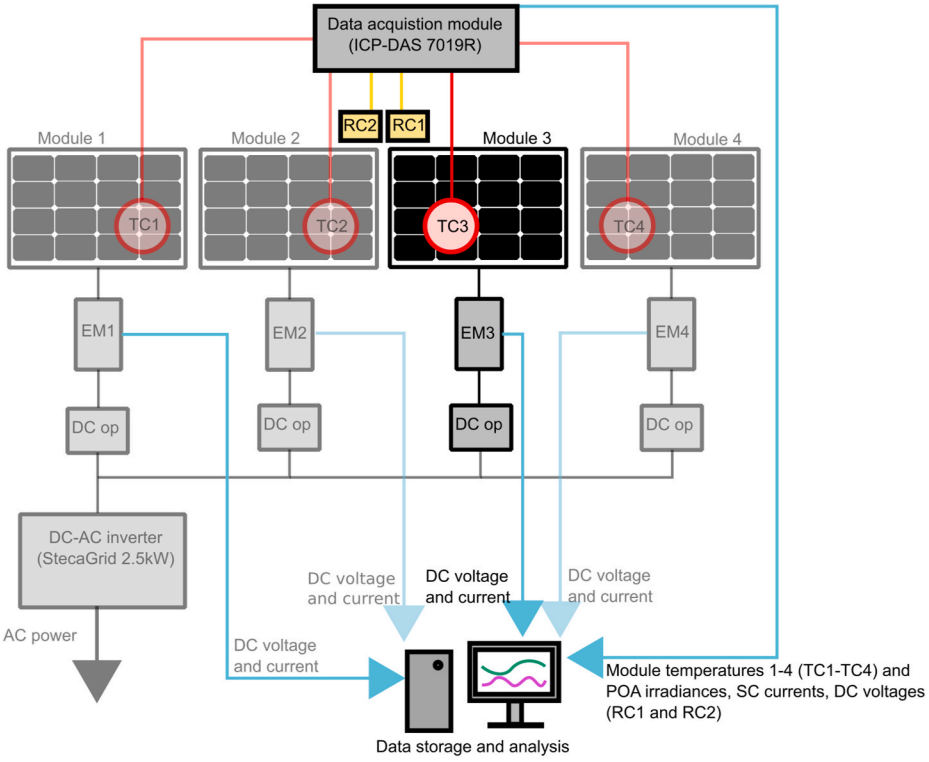

Fig. 3. Schematic diagram of the PV system setup, including the 4 solar modules, reference cell, and thermocouple connections. Abbreviations: RC=Reference cell, TC=Thermocouple, EM = Energy meter, DC op = DC-DC optimizer. The connections related to module 3 are highlighted since this study concerns data only from this module.

Table 2
Measured variables for each separate data logging system of the field system with corresponding start and end dates. Datetimes are given in UTC+02 time zone.

	EM3	RCTC	Weather
Start-end	8/18/2017–7/2/2021	8/18/2017–7/2/2021	1/3/2018–7/2/2021
Variables	Datetime	Datetime	Datetime
	DC voltage at MPP	East POA irradiance	Wind direction
	DC current at MPP	West POA irradiance	Wind speed
	DC power at MPP[a]	TC for each module	Rain
	Total energy yield[a]	SC current (for both cells)	Relative humidity
		OC voltage (for both cells)	Ambient temperature
			GHI (with two pyranometers)[b]

[a] Was not monitored directly but calculated using current and voltage.
[b] Data logging ended 9/18/2020.

annual GHI yield is presented. Regarding all values, there are little changes from year to year. On average, GHI is around 240 W/m^2, but has peaks over 1000 W/m^2. The total annual yield varies around 900-1000 kWh/m^2, with the highest value in 2018, even though there is a large gap in the weather data during the spring of 2018 (more details in SI2). This suggests that the year 2018 was especially sunny, since the yield of 2019 is lower than that, despite that there was less missing data during the year 2019. Regarding the year 2020, the removal of the pyranometer setup causes the yield to also remain distinctly lower than that of 2018. Air temperature has a mean close to 10 °C, but ranges between −20 °C and 30 °C (year 2020 has a minimum of −10 °C, because there was a monitoring gap during the coldest winter time). Considering the location of this setup, the wind speed was around 2 m/s on average, and never exceeded 10 m/s during the monitoring period.

2.3. Irradiance and temperature modeling

Since POA irradiance is monitored from both sides separately, effective bifacial POA irradiance is used as the incident irradiance, given by the following equation [46]:

$$G_{E,BPV} = G_{front} + BF \times G_{rear}, \quad (1)$$

where G_{front} and G_{rear} are the front and rear POA irradiances, respectively, and BF is the bifaciality factor, defined as the fraction of rear and front side efficiencies. For the given module [42], $BF = 0.90$. The effective bifacial irradiance corresponds to a situation where all incident irradiance from both sides would be absorbed in the front side when considering the module power generation. It should be noted that the effective bifacial irradiance used here is not related to the effective irradiance introduced by Sandia [47], which accounts for angle of incidence losses, soiling, and spectral mismatch.

The cell temperature is calculated by applying the Sandia temperature model [47] using the module surface temperature monitored with a TC. Since the module surface temperature data of EM3 was partly faulty (more information in section SI2 in the supporting information), the module temperatures from another module located next to the EM3 were used instead. The Sandia temperature model is developed for conventionally mounted modules with TCs attached on the rear side. However, given the lack of bifacial-specific cell temperature models, many cell temperature models developed for monofacial modules are adopted for bifacial technology simply by taking into account the irradiance on both sides rather than only considering the front side irradiance [48,49], including the Sandia model. To take the heating of the TC under direct sunlight into account, the following three equations (T_{c1}, T_{c2}, and their linear combination) were used based on the given irradiance conditions:

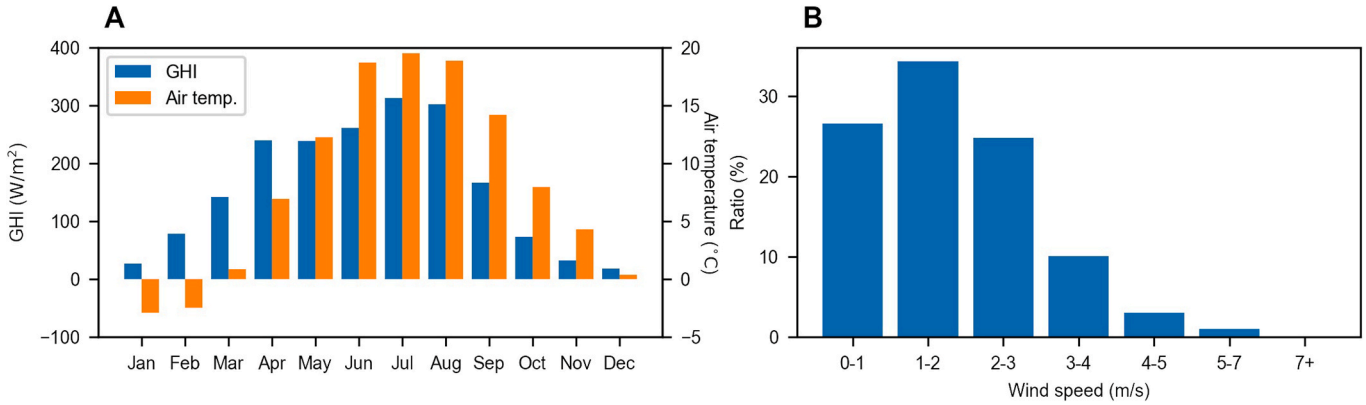

Fig. 4. A: Monthly means of global horizontal irradiance (GHI) and air temperature over the whole measuring period. B: A bar plot of wind speed distribution. All data is from the nearby weather station.

Table 3
Descriptive statistics for the raw minute-level global horizontal irradiance (GHI), air temperature, and wind speed for the monitored years. GHI values during 2021 are missing since the pyranometers were removed in September 2020.

	GHI (W/m^2)				Air temperature (°C)			Wind speed (m/s)		
	Mean	Min	Max	Yield (kWh/m^2)	Mean	Min	Max	Mean	Min	Max
2018	248	0	1124	1031	11	−21	33	1.8	0.2	9.4
2019	236	0	1114	941	11	−19	33	1.7	0.2	8.9
2020	248	0	1109	942	12	−10	31	1.9	0.2	9.8
2021	–	–	–	–	7	−22	31	1.9	0.2	9.7

$$T_c = \begin{cases} T_{c1} = T_m - \dfrac{G_{front}}{G_{ref}} \times \Delta T, \text{if } G_{front} > 2 \times G_{rear} \\ T_{c2} = T_m + \dfrac{G_{front} + G_{rear}}{G_{ref}} \times \Delta T, \text{if } G_{front} \leq G_{rear} \\ T_{c1} \times \left(\dfrac{G_{front}}{G_{rear}} - 1\right) + T_{c2} \times \left(2 - \dfrac{G_{front}}{G_{rear}}\right), \text{else} \end{cases} \quad (2)$$

where T_m is the module surface temperature (front side), and ΔT is the temperature difference, defined as the difference between the cell and the back surface at $G_{ref} = 1,000$ W/m^2 in the case of conventionally mounted modules. T_{c1} is used when the sun illuminates the front side of the module. In that case, the temperature of the TC is likely higher than the cell temperature, which is compensated by subtracting ΔT from the T_m instead of adding it. When the irradiance on the rear side is greater than on the front side, the TC is on the opposing side than the sun (and thus effectively on the back side of the module). In that case, the regular Sandia cell temperature model T_{c2} is applied using the sum of the front and rear irradiances. Since both sides absorb light, irradiance from both sides affects the heating of the cells inside the module. When the front side irradiance is slightly greater than the rear side irradiance, either the sun is close to the solar noon or the sun illuminates from the front side under overcast conditions. In that case, a linear combination of T_{c1} and T_{c2} is used to account for the possible heating of the TC as well as the heating of the cells. Although the module temperature T_m in the Sandia model [47] refers to the rear side temperature, in the case of east-west mounted VBPV, the distinction between the front and rear side is arbitrary in terms of surface temperature, since both sides are under direct sunlight in turns. The value of $\Delta T = 3\ ^\circ C$ was used, which is a value for open rack glass-cell-glass and glass-cell-polymer modules provided by Sandia [47]. This value was used due to the lack of value for VBPV mounting and since its description corresponds the best with the bifacial module setup (glass-cell-glass, vertical racking).

2.4. Data filters

The data are filtered to exclude data that are non-relevant in terms of performance analysis, affected by system malfunctions, or recorded under conditions that are hard to model or not suitable for a given performance model. This includes, for instance, nighttime, sensor issues, shadows, and low irradiance conditions. The filters applied in this study are presented in Table 4. The nighttime filter excludes nighttime data based on irradiance and electrical conditions. Varying irradiance lower limits (LL) are applied to study the effect of the irradiance cutoff filter. The International Electrotechnical Commission (IEC) provides an example of the minimum threshold filtering conditions for PV and weather data [50]. Due to a lack of AC power readings, DC power is used. The front side rating is used as the power rating. The outlier filter is applied to exclude data affected by, for example, shading conditions that cause unmatched power-irradiance data. A clear-sky (CS) filter is used to exclude overcast conditions. It is applied using a clear-sky index (CSI), which is the ratio of measured GHI and modeled CS GHI. The CS filter is implemented using the PVLib package (version 0.8.1) for Python [51]. CS GHI values are calculated with the Haurwitz model [52,53]. More detailed descriptions of the filters are given in section SI3 in the supporting information.

Table 4
Filters applied in this study. Abbreviations: $G_{E,BPV}$ = Effective bifacial irradiance, V=Output voltage, I=Output current, T_{air} = Air temperature, WS=Wind speed, P_{AC} = AC power, SD=Standard deviation, P=Power, CSI=Clear-sky index.

Filter description	Filter conditions
Nighttime filter	$G_{E,BPV} \geq 5$ W/m^2 and ($V > 0$ V or $I > 0$ A)
Irradiance cutoff filter	0 W/m^2, 5 W/m^2, 20 W/m^2, 50 W/m^2, 100 W/m^2, 200 W/m^2, 500 W/m^2, 800 W/m^2
IEC filter	-6 W/m^2 $\leq G_{E,BPV} \leq 1,500$ W/m^2, -30 C $\leq T_{air} \leq 50$ C, 0 m/s $\leq WS \leq 32$ m/s, $-0.01 \times$ rating $\leq P_{AC} \leq 1.02 \times$ rating
Outlier filter	Monthly mean $\pm 2 \times$ SD of $P/G_{E,BPV}$ after applying nighttime filter
CS filter	$0.8 \leq CSI \leq 1.2$

2.5. Performance metrics

PLR is obtained statistically from performance time-series data. The performance datapoints are calculated with a performance model, which is usually based on generated power or energy yield. Calculating performance losses from power will not provide reliable results since the power generation is solely based on the ambient conditions, which varies from year to year. Thus, performance models often include weather variables, namely irradiance and temperature, to assess the actual state of the performance of PV independent of the prevailing weather conditions.

Often performance metrics utilize the module nameplate rating, such as the rated power of the module, since it is easy to access and apply. Nameplate rating is usually reported at STC (irradiance of 1000 W/m^2, spectral composition corresponding to AM1.5 and cell temperature of 25 °C) [54], and hence weather corrections are recommended to correct the measured output to STC or to correct the rated power to ambient conditions. However, there is no standardized power rating methodology for BPV due to the lack of a definition of rear side irradiance under front side irradiance of 1000 W/m^2 [55,56]. Here the front side nominal power is used as the rated power P_0 and reference irradiance of 1000 W/m^2 in all performance metrics in accordance with IEC's guidelines [57]. However, the selection of reference conditions is arbitrary as the BSTC reference conditions of 375 W and 1270 W/m^2 ($1,000$ W/m^2 + $0.9 \times$ 300 W/m^2) provide the same results regarding performance metric calculation. Below, the five performance metrics used in this study, in addition to P_{MPP}, are presented.

Performance ratio. A widely used performance metric, defined as the ratio of a system's final yield to its reference yield from a given time period, such as one day, and is calculated with the following equation [57]:

$$PR = \frac{Y_f}{Y_r} = \sum_k (P_k \times \tau_k) \Big/ \sum_k \left(\frac{P_0 \times G_k \times \tau_k}{G_{ref}}\right), \quad (3)$$

where Y_f is the final yield, Y_r is the reference yield, P_k is the system's output power, τ_k is the duration of the k^{th} recording interval within the reporting period, G_k is the POA irradiance at the k^{th} recording (effective bifacial irradiance $G_{E,BPV}$ is used as POA irradiance), and G_{ref} is the reference irradiance of 1000 W/m^2.

Temperature-corrected PR (PRt). A commonly used metric for PLR calculation, and its advantage over regular PR is the inclusion of cell temperature, which affects module efficiency. PRt is calculated with the following equation [57]:

$$PRt = \frac{Y_f}{Y_{r,t}} = \sum_k (P_k \times \tau_k) \Big/ \sum_k \left(\frac{C_k \times P_0 \times G_k \times \tau_k}{G_{ref}}\right), \quad (4)$$

where $Y_{r,t}$ is the temperature-corrected reference yield, and the temperature correction C_k is given by the equation

$$C_k = 1 + \gamma \times \left(T_{cell,k} - T_{ref}\right), \quad (5)$$

where γ is the temperature coefficient of power, $T_{cell,k}$ is the cell temperature in time interval k, and T_{ref} is the STC temperature of 25 °C.

Power performance index (PI). A ratio of measured output to expected output, which is calculated using a performance model and measured weather data [57]. Here, PI is calculated on the basis of

power, and as a performance model, the PVWatts model is used, given by the following equation [58]:

$$P_{expected} = P_0 \times \frac{G}{G_{ref}} \times C_k. \quad (6)$$

Thereby, the power-based PI used in this study is given as the following ratio:

$$PI = \frac{P_{measured}}{P_{expected}} = \frac{P_{MPP}}{P_0 \times \frac{G}{G_{ref}} \times C_k}. \quad (7)$$

This is very similar to PRt, and the separating factor is that PRt is calculated using energy yields and PI using instantaneous powers.

PVUSA. A commonly used regression-based power rating model developed as a part of the Photovoltaics for Utility Scale Applications (PVUSA) project, given by the following equation [59]:

$$P = G \times (a + b \times G + c \times T_{air} + d \times WS), \quad (8)$$

where $a - d$ are regression coefficients, G is POA irradiance, T_{air} is air temperature, and WS is windspeed. The model predicts the output power at given ambient conditions without any system-related parameters. The model is developed for c-Si technology, and it is reported that PVUSA has an increasing error when irradiance decreases to below 500 W/m^2, thus it is recommended to exclude datapoints with irradiance below 500 W/m^2 [59].

Here, PVUSA is applied by fitting Eq. (8) separately to daily, weekly, or monthly blocks to obtain the regression coefficients and using the corresponding coefficients to calculate daily, weekly, or monthly powers at PVUSA Test Conditions (PTC, $G = 1,000$ W/m^2, $T_{air} = 20$ C, and $WS = 1$ m/s [59]). The regression fits are obtained using non-linear least squares implemented with a *curve_fit* function (from the module *optimize*) of the SciPy library (version 1.8.0) for Python.

6k. A power-predictive regression model, given by the following equation [60]:

$$\begin{aligned} P(G^{'}, T^{'}) &= G^{'} \times \left[P_0 + k_1 \times \ln(G^{'}) + k_2 \times \ln(G^{'})^2 + k_3 \times T^{'} + k_4 \times T^{'} \times \ln(G^{'}) + k_5 \times T^{'} \times (G^{'})^2 + k_6 \times T^{'2}\right], \\ G^{'} &\equiv G/G_{ref}, \\ T^{'} &\equiv T_{cell} - T_{ref}, \end{aligned} \quad (9)$$

where $k_1 - k_6$ are the regression coefficients. Based on the coefficients, the model predicts the output power at given irradiance and temperature conditions. The 6k model is applicable solely for c-Si modules, and it has proved good accuracy down to a POA irradiance of 50 W/m^2 [60].

In this study, performance losses are calculated by first obtaining the regression coefficients by fitting Eq. (9) to filtered data from 2018. Then, measured power values are divided by the predicted values. The year 2018 was chosen as the training year since it has continuous PV and RC data recordings (the weather station data are not used as an input in the model).

Module efficiency. A measure of performance which indicates the module's ability to convert light to electricity. Apart from the rest of the performance metrics presented above, the efficiency is not used in PLR calculation, but is used to illustrate its dependency of irradiance (in section 3.2.) The normalized module efficiency is calculated using the equation

$$\eta = \frac{P_{MPP}}{P_0 \times \left[1 + \gamma \times \left(T_{cell} - T_{ref}\right)\right]} \times \frac{I_{MPP,STC} \times \left[1 + \alpha \times \left(T_{cell} - T_{ref}\right)\right]}{I_{MPP}}, \quad (10)$$

where α stands for the temperature coefficient of current, P_{MPP} and I_{MPP} stand for power and current at MPP, respectively, and $I_{MPP,STC}$ stands for current at MPP under front side STC conditions (see Table 1). This equation is modified from Ref. [61], where short circuit currents are used instead of MPP currents. However, since the short circuit current was not monitored, MPP currents were used. This approximation is sufficient because efficiency is used only to illustrate a phenomenon, not to determine quantitative values.

2.6. Statistical models for calculating PLR

In this study, three different methods are applied to obtain the PLR: least squares linear regression (LSLR), robust regression, and year-on-year (YOY). The first two of the three methods are linear regression methods, widely used in different research applications, while the third is specifically developed for performance loss analysis. Below, the statistical models are further described.

Least squares linear regression. In terms of PLR, performance is assumed to decrease linearly as a function of time. Therefore, PLR can be obtained by fitting a linear regression between the performance metric data and elapsed time. Least squares linear regression (LSLR) is the most popular type of linear regression, and it is based on the minimization of the squared error of residuals. PLR is calculated using the slope and the vertical intercept of a regression fit, given by the following equation [11]:

$$PLR[\%/year] = \frac{a}{b} \times t \times 100, \quad (11)$$

where a is the slope, b is the vertical intercept of the linear model on performance time-series data (y-axis: performance, x-axis: elapsed time), and t is the number of datapoints per year (e.g., 12 for monthly data and 52 for weekly data).

Robust regression. LSLR is highly sensitive to outliers due to the optimization based on squared errors. To increase the robustness against outlying values, robust regression models can be used. Here, Huber's M-estimation is used, where the loss function to be minimized is quadratic for residuals close to the corresponding predicted values and linear for residuals far from the predicted values [62]. The regression is implemented using the Statsmodels library (version 0.14.0) for Python. In this study, this robust regression model is referred to as robust linear regression (RLR).

Year-on-year. YOY is a method for PLR assessment developed by Hasselbrink et al. [63]. Instead of calculating one value for the loss rate, YOY provides a distribution of rates (referred to here as "YOY distribution"), of which the average value represents the overall long-term PLR. The distribution is obtained by calculating the loss in performance between two points one year apart and performing this for all datapoints. YOY is more robust to outliers and seasonal patterns compared to regression models [22] because the performance comparisons are conducted using two datapoints taken from the same time of the year. Here, YOY is applied using the RdTools library (version 2.1.3) [27].

3. Results and discussion

3.1. Data quality

The quality of the data was evaluated using the data quality grading criteria by Lindig et al. [11], which ranks the data from A to D (A being the highest category) in terms of the percentage of data outliers, missing data, and the longest gap in the data. Using these grading criteria to the

analyzed datasets, the gradings for outliers, missing data, and longest gap are A, A, and C, respectively, indicating that the data are of high quality. The main issues in data quality were two larger gaps in the power data, the longer being 1.5 months long and TC2 introducing faulty temperature readings. However, the two gaps have an insignificant effect on the long-term performance and PLR analysis, and the corrupted temperature data were handled by using temperature readings from TC3. A more detailed description of the data quality grading and quality issues is presented in section SI2 in the supporting information.

3.2. Effects of filtering and performance metrics on data

To gain an understanding of the distribution of incident irradiance, the data are divided into various $G_{E,BPV}$ ranges in Fig. 5. In Fig. 5A, the module output power is presented as a function of $G_{E,BPV}$ with different irradiance ranges. Nighttime datapoints are filtered beforehand, resulting in the lowest $G_{E,BPV}$ of 5 W/m^2. In Fig. 5B, a bar plot displaying the percentage of datapoints corresponding to each irradiance range is presented. These graphs highlight that most of the datapoints lie in the low irradiance area under 200 W/m^2. Thus, removing data even under 200 W/m^2 (a common cutoff threshold) would exclude a large proportion of data, possibly affecting the accuracy of PLR [9,16], and hindering the analysis of performance loss patterns, due to the long continuous gaps during winters (see section SI4 in supporting information for further information).

In Fig. 6, the effects of IEC's recommended minimum threshold filters (Fig. 6A), outlier filter (Fig. 6B), and CS filter (Fig. 6C) on the data are illustrated. Nighttime datapoints are excluded before applying the different filters and calculating percentages. The IEC filter has only a very minor effect on the data, thus power-irradiance outliers will be included into further PLR calculation steps. The outlier filter effectively eliminates data that fail to follow the near-linear relationship of power and irradiance with only a small fraction of datapoints filtered, visible in Fig. 6B. As can be seen from Fig. 6C, the CS filter, alternatively, handles the power-irradiance outliers insufficiently and filters out almost 60% of the daytime datapoints. Although a large percentage of data is removed, the removed data correspond to only 30% of the total power production, implying that the removal of data relevant for performance analysis is moderate. The CS filter passes only datapoints corresponding to clear periods, and as presented later in section 3.4, this selection might introduce bias in the calculated PLR.

One considerable effect the IEC and CS filters have on the data is the change in the length of the time series. Since the different data sources have different recording intervals (namely weather data and GHI compared to the EM3 and RCTC datasets), applying the IEC and CS filters shortens the length of data to 3.5 and 2.7 years, respectively (data recording intervals are presented in Table 2).

Power (P_{MPP}), PR, PRt, 6k, PVUSA, and PI were used as performance metrics in this work. To study these metrics, their time series are presented in Fig. 7A–F, respectively. The outlier filter with the nighttime filter is used, and the data are presented with daily and monthly aggregation. All metrics reduce the variation compared to the power, which has a very distinct seasonal pattern. Low powers during the winters are due to the low irradiance conditions. This sensitivity to ambient conditions highlights the importance of including weather corrections in performance assessment.

Considering the time series, PRt (Fig. 7C) has surprisingly more apparent seasonal patterns compared to regular PR (Fig. 7B). More precisely, the noisy time series of PR becomes very regular and seasonal when temperature correction is implemented using the temperature coefficient. A similar seasonal shape is apparent when using PI (Fig. 7F), which also implements the temperature correction based on the temperature coefficient. These similar patterns suggest that the widely used temperature correction based on the temperature coefficient is insufficient during winter conditions in Nordic areas or that there are other effects that reduce the power output during winters. Because irradiance is monitored via an RC, the effects of changing the spectrum or angle of incidence should be minimal. However, it has been observed that the dependency of power on cell temperature varies with irradiance in outdoor conditions [64–67] and that the conversion efficiency decreases during low irradiance conditions [61]. It is important to acknowledge how significantly the temperature corrections distort the PR data in Nordics.

The occurrence of these two effects is verified in Fig. 8. In Fig. 8A, power is presented as a function of cell temperature with various effective bifacial irradiances, using data from the first year that is recorded in the morning before midday, to minimize the scattering (data after midday has a similar behavior but introduced more noise). Linear regression was applied to each set of datapoints to obtain the slopes, which correspond to the temperature coefficients of powers at different irradiances. In Fig. 8B, these coefficients are presented as a function of $G_{E,BPV}$, resulting in an apparent linear relationship. When a linear regression line is fitted to these data, extrapolation to the reference irradiance of 1000 W/m^2 provides a temperature coefficient of −0.416 %/°C, which is very close to the coefficient provided by the manufacturer (−0.414 %/°C). Previous studies suggest that the temperature coefficient obtained from outdoor data is affected by various effects such as uneven temperature distribution, the module's heat capacitance,

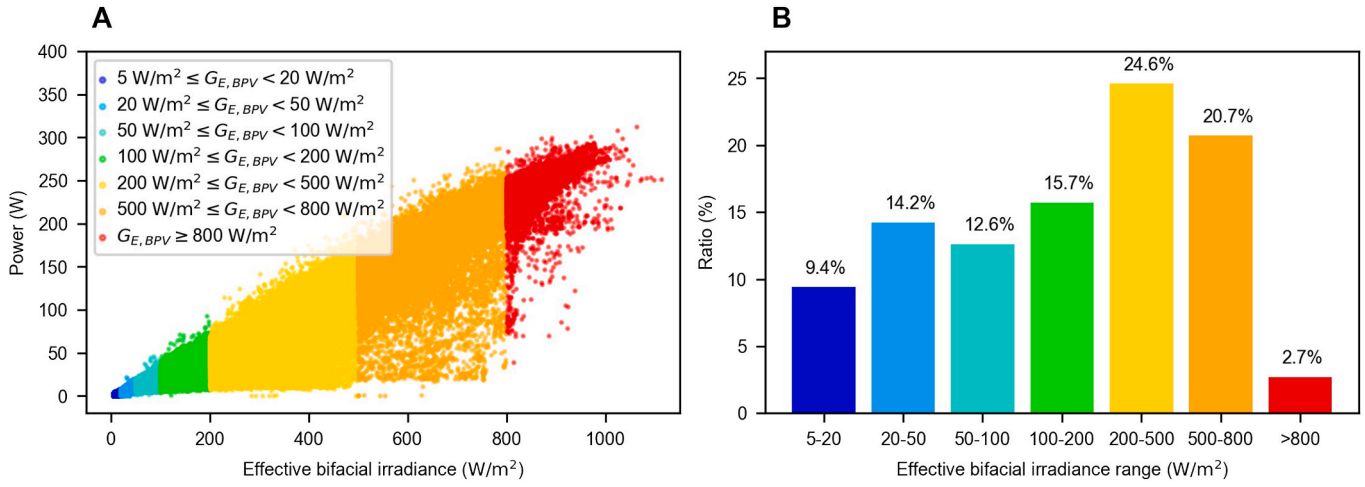

Fig. 5. A: Power vs. effective bifacial irradiance ($G_{E,BPV}$) with various irradiance ranges. B: The ratio of the remaining dataset size to the whole daytime dataset size for a given irradiance range. Nighttime data are excluded.

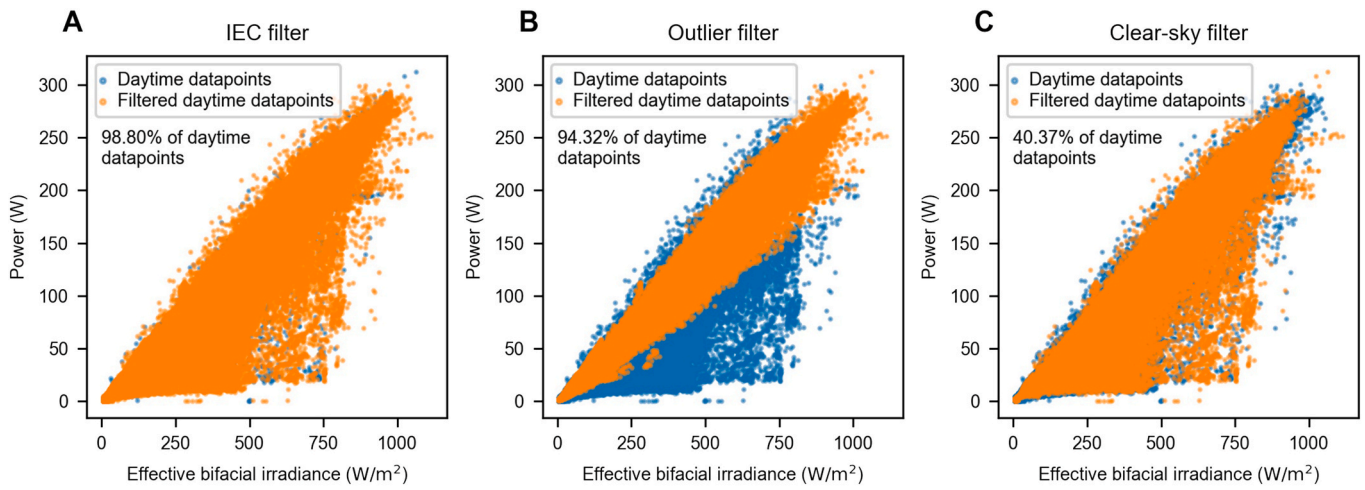

Fig. 6. Power vs. effective bifacial irradiance graph when A: the IEC filter, B: the outlier filter, and C: the clear-sky filter are applied.

spectral conditions, and incidence angle [65,68,69], and that it is very system-specific [70]. Thus, the temperature coefficient obtained from outdoor data is rather an "effective" temperature coefficient [68]. In Fig. 8C, the normalized efficiency of the module is presented as a function of $G_{E,BPV}$, using data collected in the first year. Based on the red trend line (a moving average), the normalized efficiency is around one when irradiance is over 300 W/m^2 but decreases as the irradiance further decreases. Under an irradiance of 100 W/m^2, the efficiency drops to zero. This change in efficiency is not assumed in the PR, PRt, or PI models, which all assume a linear relationship between power and irradiance. At least these two effects (varying "effective" temperature coefficient and low irradiance losses) contribute to the seasonal behavior since they are not included in the PRt or PI formulas (Eq. (4) and Eq. (7)).

From the two regression-based performance metrics in Figs. 7 and 6k results in a very stable trend without any noticeable seasonal patterns (Fig. 7D), whereas PVUSA introduces consistent anomalies during winters (Fig. 7E), which indicates its weakness regarding low irradiance/low temperature conditions. In addition to the actual regression models, the fitting practice of the models should be acknowledged. 6k is trained using one year of data, which should help the model learn the effects of different weather conditions. PVUSA is fitted to the daily, weekly, or monthly interval blocks separately, in which case the number of training data can be very small, resulting inaccurate fits and outlying values when performance is extrapolated to PTC conditions. These results align with another study, which also demonstrated that PVUSA can perform poorly when applied to data far from PTC [10].

Of the studied performance metrics, those that include temperature and irradiance effects, namely PRt, PI, PVUSA, and 6k, all behave similarly: they result in consistent and stable performance values near 1.0 during summer, but during winter they introduce anomalies. This verifies that the often applied metrics do not apply in the full range of operating conditions. Of all the metrics, 6k results in the least seasonal variation, especially when data are aggregated to monthly values. This low variability indicates its ability to account for weather effects in a wide range of conditions. What separates it from the rest of the metrics is its regression-based training on varying weather conditions and its ability to handle losses due to the low irradiance conditions, at least down to 50 W/m^2, as reported [60]. Especially the complex fitting regression, given in Eq. (9), could help learn seasonal patterns, such as the low irradiance losses and changes of temperature dependency as well as possible seasonal soiling, etc. This regression fitting might be the reason there is considerably less seasonal variability when 6k is applied.

3.3. Estimating real PLR

When comparing different PLR calculation approaches, they should be validated against the "real" performance loss of the module. Instead of using flash tests for performance loss evaluation, Lindig et al. [11] proposed an ensemble method for estimating the real PLR ($\overline{PLR}$) from multiple PLR values obtained with different approaches, that is, filter-metric-aggregation-model combinations. As each PLR calculation approach affects the PLR differently, PLR values vary around the real underlying PLR, which can be estimated as the mean of the multiple PLRs. As more approaches are used, the confidence of the mean should increase [11].

In this study, PLRs calculated with different filter-metric-aggregation-model combinations result in over 1600 values, ranging from −346 %/year to +2661 %/year, implying that there are blatant outliers. Combinations where POA LL is 800 W/m^2 are excluded since this filter creates bias in PLR, which is covered in section 3.4. The outlying PLR values are removed based on the interquartile range (IQR), which is the distance between the first quartile and the third quartile of the data: all values outside the (first quartile −1.5× IQR) and (third quartile +1.5× IQR) are excluded in accordance with common statistical practices [71]. Concisely, PLRs located far from the densest area around the middle are removed. The histogram of remaining about 1200 PLR values is presented in Fig. 9. PLRs are approximately normally distributed, in which case the mean value can be used as an reliable estimate [72]. The mean of the remaining values is −1.46 %/year, and it represents the $\overline{PLR}$. As for the error of this estimate, the standard error of the mean with a confidence level of 95% is calculated to quantify the uncertainty of this estimate [73]. Therefore, the estimated PLR of the module is $\overline{PLR} = (-1.46 \pm 0.03)$ %/year, indicating over 40% performance loss in 30 years, which is over twice as much as the manufacturer guarantees (20% power loss in 30 years). Considering crystalline silicon modules/systems in general, this value is rather high since the PLRs have been reported to be well under −1.0 %/year when located in snowy climates [74]. However, the high PLR of −1.8 %/year for the bifacial system reported by Mannino et al. [35] aligns with the results of this work. More studies need to be carried out to verify whether bifacial modules have faster degradation compared to monofacial modules. The PLR could be high due to an infant phase degradation mode, such as potential induced degradation [75,76], and the performance loss may slow down in the following years [77]. In that case, approximating the performance losses during the lifetime of the module using this value could be erroneous. Additionally, soiling of the module could contribute to the high value to some extent, although VBPV modules have been reported to hardly suffer from soiling [44].

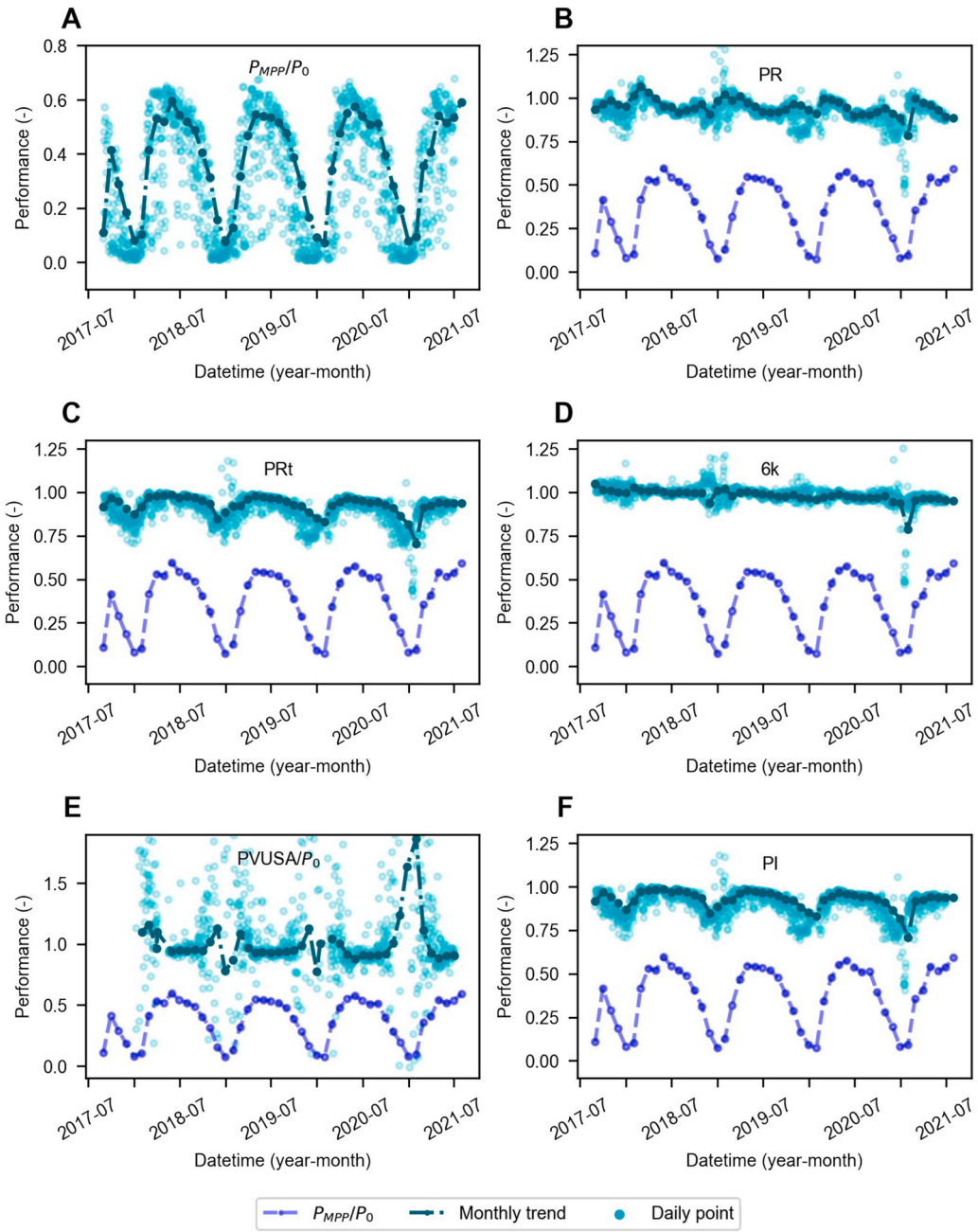

Fig. 7. Monthly and daily datapoints of different performance metrics: A: power, B: performance ratio, C: temperature-corrected performance ratio, D: 6k regression methods, E: PVUSA regression methods, F: performance index. As filtering conditions, the nighttime filter with the outlier filter are used. To have the same scale, power and PVUSA were normalized by front side power rating P_0.

3.4. PLR under varying conditions

The effects of varying irradiance conditions on PLR was examined to discover possible biases due to varying weather conditions. In Fig. 10, PLRs are presented as a function of $G_{E,BPV}$ range using various performance metrics and two aggregation-model combinations for verification: 6k, PRt, PI, and PR, and daily YOY (Fig. 10A) and monthly RLR (Fig. 10B). Neither outlier nor CS filter is applied here. Both aggregation-model combinations display similar behavior with all metrics: low irradiances result in the highest PLRs, which decrease as irradiance increases. This pattern is more distinct when YOY is used, while the RLR introduces more scattering, likely due to the RLR's sensitivity to outliers. Irradiances under 5 W/m^2 are mostly nighttime data, causing the corresponding PLRs to deviate largely. The low PLR obtained with high irradiance over 800 W/m^2 is caused by the bias of the front side data over the rear side data.

The results of Lindig et al. [11] suggest that this irradiance dependency of PLR could be caused by the decrease in shunt resistance, which affects the performance particularly at low irradiance conditions. However, the cause of this phenomenon is out of the scope of this study, but it is important to be aware of the existence of this effect when calculating PLR. These results imply that the PLR calculated from the full range of conditions could be higher compared to flash test results obtained from STC. Furthermore, measuring the quantum efficiency of solar modules before and after the outdoor testing would be helpful in identifying whether there are wavelength-dependent changes in the module performance.

In addition to different irradiance ranges, CS and overcast conditions

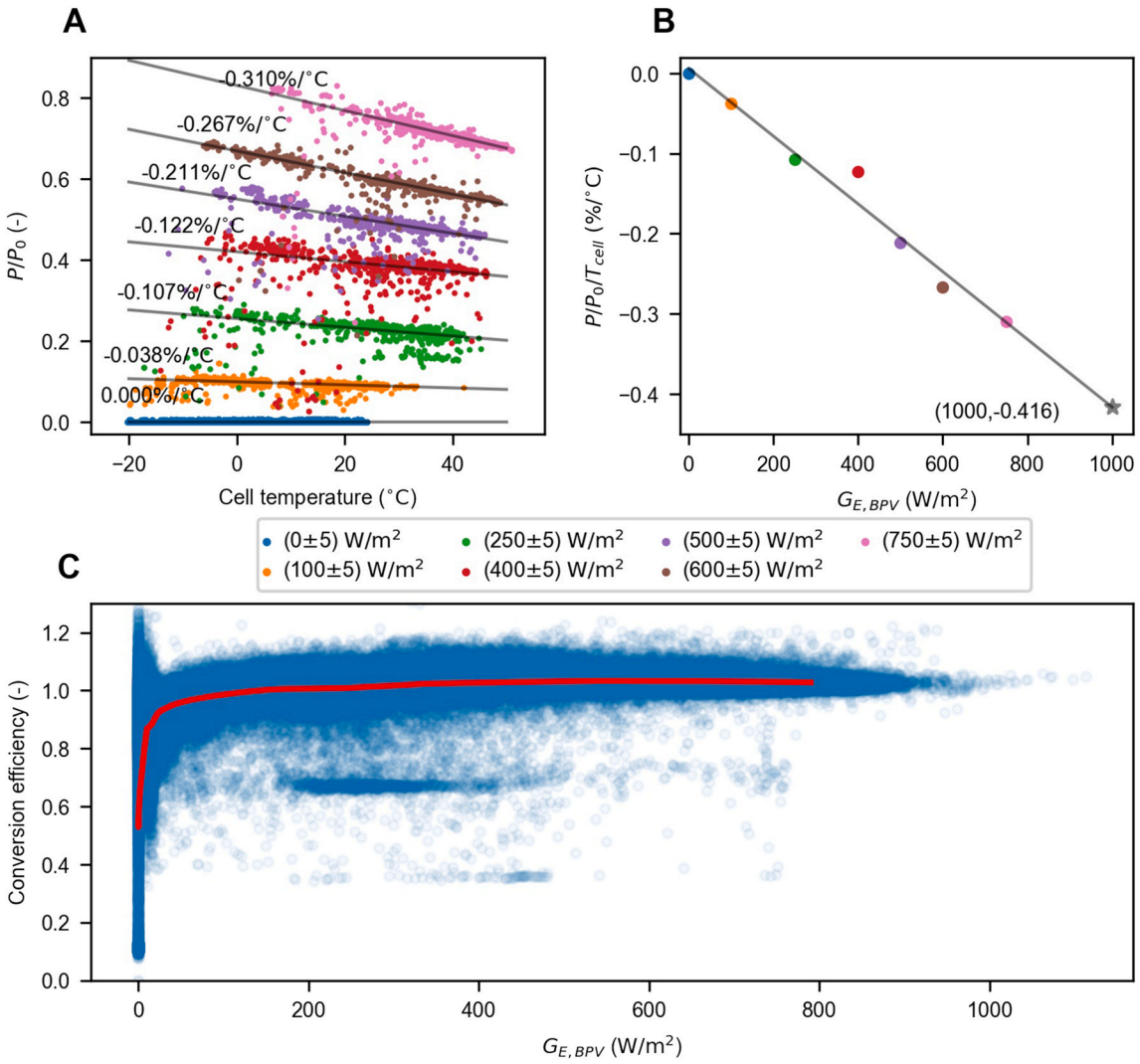

Fig. 8. A: Normalized power during the first operation year (using morning data before 12 p.m.) as a function of cell temperature with various effective bifacial irradiance ($G_{E,BPV}$) ranges, and linear fits presenting the temperature dependency of power. B: The temperature coefficients for different $G_{E,BPV}$ ranges as a function of $G_{E,BPV}$ and a linear fit. C: Normalized efficiency of the module as a function of $G_{E,BPV}$ during the first operation year. The red line shows the moving average of the efficiency values. Abbreviations: P=Output power, P_0=Rated power, T_{cell} = Cell temperature.

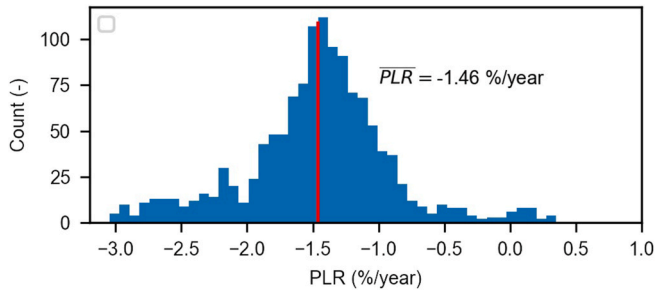

Fig. 9. A histogram of PLR values when outlying PLRs are filtered out. The red line corresponds to the estimated PLR ($\overline{PLR}$), which is the mean of the histogram values.

result in varying PLRs. This variance is illustrated in Fig. 11A using monthly PRt and a POA LL of 500 W/m^2. PRt values are separated into CS values and overcast values by using the CS filter, and PLRs are obtained with LSLR. The time range is limited to under three years due to the monitoring period of the weather dataset, which is used for CS filtering. The PLR under CS conditions is noticeably higher compared to the PLR under overcast conditions, suggesting that PLR varies under different illumination conditions (namely direct and diffuse illumination). Many different filter-metric-aggregation-model combinations were tested with comparable results.

In Fig. 11B, monthly PRt points with the POA LL of 500 W/m^2 are presented separately into data collected before noon and after noon (noon referring to midday, 12 p.m.). PLRs are obtained with LSLR, resulting in a pre-noon PLR of −0.49 %/year and a post-noon PLR of −2.47 %/year. This difference is highly likely due to a degradation mode specific to glass-on-glass bifacial technology, such as potential induced degradation on the rear side [78]. Datapoints are divided based on the time of the day in relation to noon, but this division corresponds well with front side- and rear side-dominated data given the hourly averaged POA irradiances in Fig. 11C. Since front side POA dominates pre-noon, the power generation is dominated by the front side, and the equivalently increased rear side POA post-noon implies dominating rear side power generation. Since the POA limit is applied to effective bifacial irradiance (Eq. (1)) which weights the rear side less, the high limit of 800 W/m^2 excludes a greater amount of rear side data compared to front side data (the remaining data have over five times more datapoints recorded before noon than after noon). Therefore, the front side effects are more dominant when performance metric values are calculated and

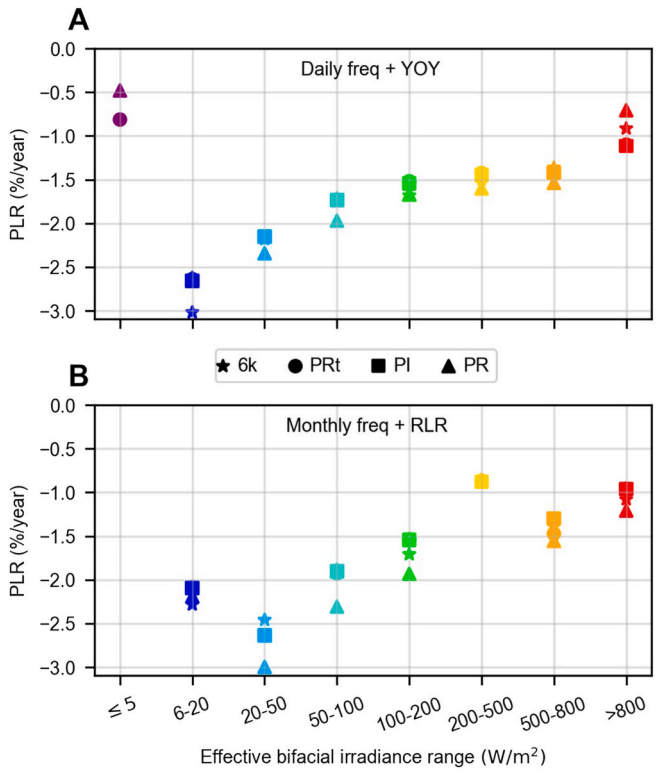

Fig. 10. Performance loss rate (PLR) values calculated under various irradiance ranges and performance metrics, when A: the year-on-year (YOY) method is applied to daily aggregated data and B: robust linear regression (RLR) is applied to monthly aggregated data.

aggregated, and consequently PLR is lower. Although other POA LLs also bias the PLR, the high LL decreases the PLR due to giving more weight to the front side performance, and therefore approaches with a POA LL of 800 W/m^2 are excluded from the PLR analysis. After all, the aim of this study is to investigate the operation of the whole module without separating the two sides.

3.5. *Effects of combined methods on PLR*

To study the accuracy and consistency of the PLR calculation approaches, individual YOY-based PLR values are presented in Fig. 12. PLRs are separated by aggregation frequency into daily, weekly, and monthly windows. Similar regression-based results are presented in the supporting information in section SI6. Regarding the regression-based PLRs, the POA LL of 500 W/m^2 with the outlier filter provide somewhat consistent and accurate results, since they reduce the seasonality and noisiness of the data. However, the regression-based PLRs are generally very scattered and with low consistency compared to the YOY results.

Considering the YOY result in Fig. 12, PLRs calculated with daily aggregation show consistency and accuracy despite the different filtering conditions, excluding PVUSA and P_{MPP}. Weekly PI and PRt show even higher accuracy and consistency, probably because the noisiness of the time series is decreased by the data aggregation. However, monthly aggregation leads to more scattered results, which is highly likely due to the statistics-driven approach of YOY. The reported loss rate of the YOY method is an average of the YOY distribution, which in most cases follows nearly a Gaussian distribution. Therefore, when there are only few datapoints in the distribution, the estimate might be unreliable.

The higher consistency and accuracy of PI and PRt over the 6k model with different filters and especially weekly aggregation is unexpected, since the 6k model was perceived to be the most suitable for varying

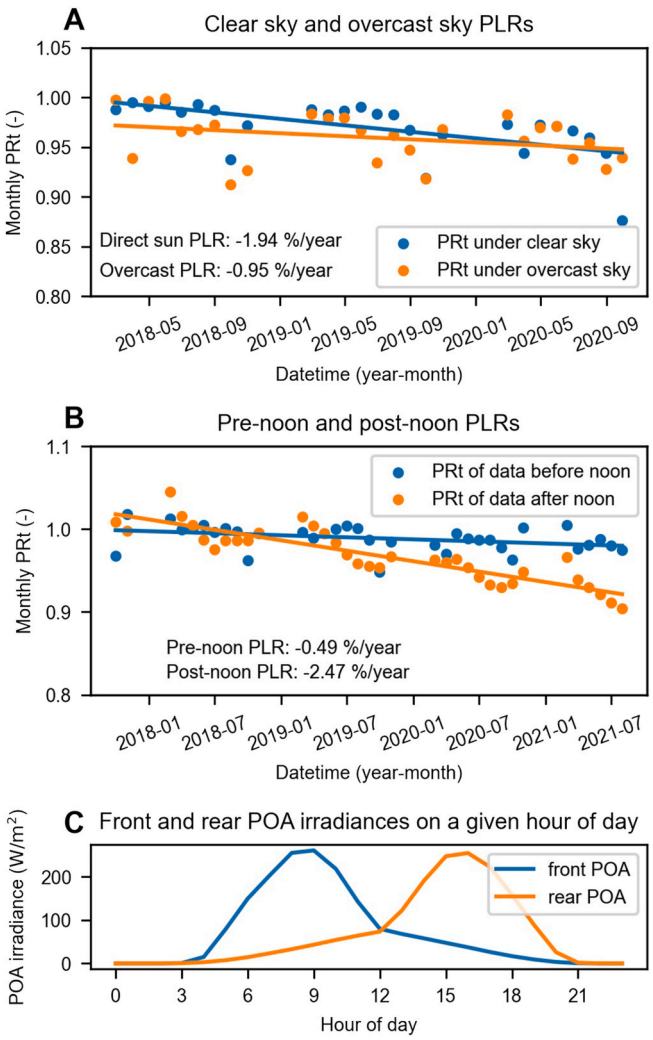

Fig. 11. Monthly aggregated PRt values with an irradiance lower limit (LL) of 500 W/m^2, with linear fits showing the PLRs for A: under clear-sky and overcast conditions separately, and B: for pre-noon (before midday) and post-noon (after midday) separately. C: Hourly averages of front and rear side plane-of-array (POA) irradiances when data from the whole measurement period are used. All data are in UTC+02 time zone.

weather conditions among the studied six performance metrics (Fig. 7). Daily aggregated 6k values lead to somewhat consistent PLRs that are mostly within ±10% of the $\overline{PLR}$, but weekly and monthly PLRs show large deviation, although the weekly and monthly 6k time series show very little seasonal variability. This increased variability suggests that 6k with YOY is sensitive to filtering when data is aggregated to weekly or monthly data. Considering regression-based results (in section SI6), 6k provides better accuracy and consistency compared to other metrics when the outlier filter is applied, which is expected due to the high linearity of the 6k time series. These results emphasize that one should focus on the synergies of a filter-metric-aggregation-model combination rather than focusing on one individual method when choosing the methods for calculating PLR.

The PLRs of PVUSA and P_{MPP} are mostly out of the range of Fig. 12, suggesting their poor suitability in PLR calculation with the given data. The unsuitability is caused by the large deviations in the performance data, visible in the performance time series (Fig. 7). Power inherently deviates because of varying weather conditions, whereas PVUSA introduces variability since the regression model is insufficient for this type of data, especially due to the large portion of irradiance conditions under 400 W/m^2. These large variabilities in the performance time

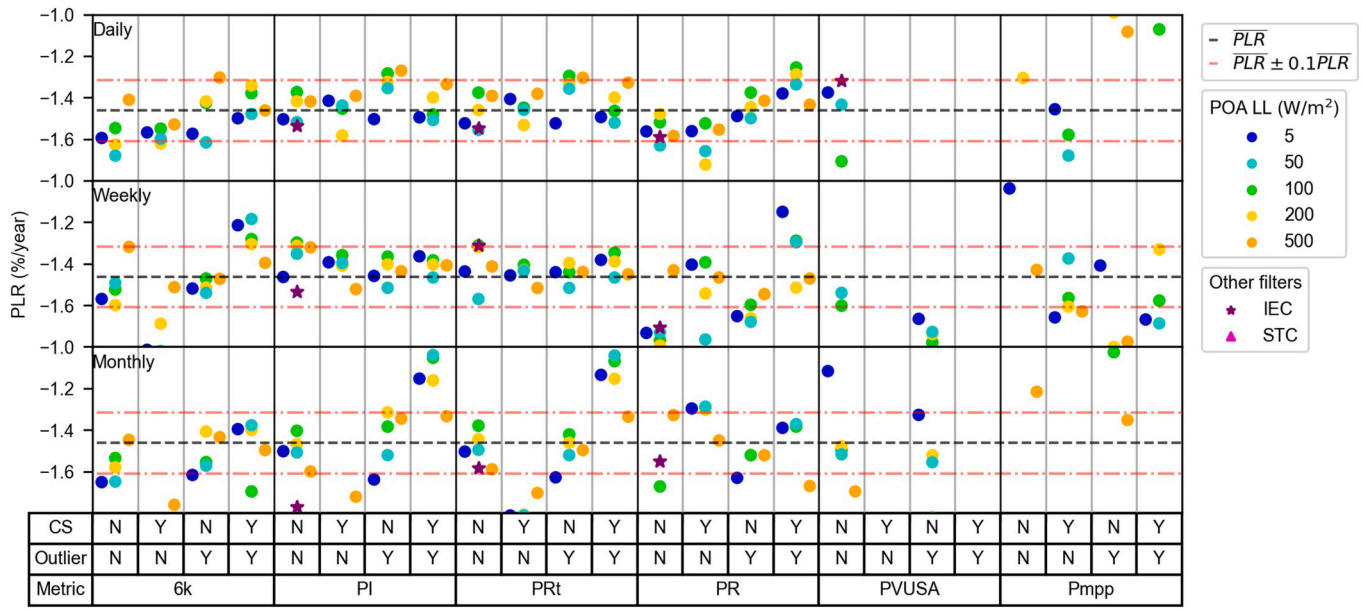

Fig. 12. Performance loss rate (PLR) values obtained with the year-on-year (YOY) method and various filter-aggregation-metric combinations. The black lines correspond to the PLR estimate $\overline{PLR}$, and the red lines $\pm 0.1 \times \overline{PLR}$ are guides to the eye. Abbreviations: POA LL=Irradiance lower limit, IEC=IEC filter, STC=STC filter, CS=Clear-sky filter, 6k=6k regression model, PI=Performance index, PRt=Temperature-corrected performance ration, PR=Performance ratio, PVUSA=PVUSA metric, Pmpp=Power at maximum power point, N=No, Y=Yes.

series increase the sensitivity of the PLR value to other methods, such as filtering and data aggregation, thus providing inconsistent results in general. From Fig. 12, it is apparent that the STC filter is unsuitable for this data, since all the STC filtered PLRs are also out of the given axis range. This is because there are very few datapoints that are passing the STC filter criteria, leading to unreliable PLR values. The IEC filter does not provide better consistency or accuracy compared to nighttime filter (POA LL of 5 W/m^2). Although it was earlier illustrated that the PLR is biased under different irradiance conditions, these biases are hardly apparent in Fig. 12.

These results display that the different approaches have a major effect on the calculated PLR. In one hand, possible underlying irradiance-dependencies have minimal effect on the PLR, but on the other hand, seemingly similar methods can produce highly varying results, such as when a POA LL of 5 or 50 W/m^2 is used and when different data aggregation frequencies are used. Additionally, a performance metric resulting in time series with little seasonal oscillation does not necessarily imply reliable PLR values, as is in the case with the 6k metric.

4. Conclusions

This work presents a four-year minute-resolution dataset from VBPV modules and an adjacent weather station in Nordic conditions, and compares an extensive amount of different PLR calculation methods to determine how the PLR for VBPV in Nordics can be calculated reliably. The PLR values obtained with different methods had considerable variation. The mean of over 1200 PLR values, -1.46 ± 0.03 %/year, is set as a benchmark, representing the real PLR of the module under the first four years of operation. However, this value is likely to decrease since performance loss is often more rapid in the early phase [74,77].

The YOY method with PI and PRt provided the highest consistency and accuracy in PLRs when applied to daily or weekly aggregated data regardless of the filtering combination. Unexpectedly, the 6k metric provided less accurate and consistent PLRs than PI or PRt when YOY was used, although the 6k model showed the least seasonal variation in the performance time series. Linear regression approaches provided very inconsistent values in general. Additionally, several widely used methods, such as PVUSA, produced very unrealistic results. More surprisingly, all performance metrics introduced inconsistencies during winter due to low irradiance and temperature conditions, highlighting that the current models perform largely insufficiently in these conditions. The lowest seasonal variability of the 6k time series suggests that of all performance metrics included in the study, 6k is best suited for the full range of outdoor conditions. Despite this linearity of 6k time series, the PLR values were inconsistent when data filtering and aggregation were varied. This result highlights the importance of analyzing the combinations of methods rather than focusing on individual methods, when calculating PLRs. Different irradiance conditions were observed to result in different PLRs—the lower the POA irradiance, the higher the PLR. Moreover, the PLR under CS conditions was higher than under overcast conditions. In addition, the results suggested that the front and rear sides of the module have highly differing PLRs. These phenomena resulted in bias in PLR.

The results of this study are expected to be applicable to other high-latitude areas apart from the Nordics since the biggest factors affecting the results are the low irradiance conditions and high seasonal variation. The key findings highlight the importance of (1) the careful data treatment, (2) the choice of the most suitable PLR calculation methods, and (3) the ensemble approach when estimating PLR, to achieve reliable results and to develop PLR calculation standards that work globally.

Data availability

Datasets related to this article can be found at https://nerc.turkuamk.fi/data-portal/, an open-source online data repository hosted by TUAS [45].

CRediT authorship contribution statement

Lauri Karttunen: Conceptualization, Methodology, Software, Formal analysis, Data curation, Writing – original draft, Writing – review & editing, Visualization. **Sami Jouttijärvi:** Conceptualization, Methodology, Writing – original draft, Writing – review & editing, Supervision. **Aapo Poskela:** Conceptualization, Writing – original draft. **Heikki Palonen:** Writing – review & editing, Supervision. **Hugo Huerta:** Investigation, Resources, Data curation. **Milica Todorović:**

Conceptualization, Writing – review & editing, Supervision. **Samuli Ranta:** Investigation, Resources. **Kati Miettunen:** Conceptualization, Writing – review & editing, Supervision.

Declaration of competing interest

The authors declare that they have no known competing financial interests or personal relationships that could have appeared to influence the work reported in this paper.

Acknowledgements

AP thanks the Jenny and Antti Wihuri Foundation (PoDoCo Post-Doc Pool), and SJ thanks the Finnish Cultural Foundation and Emil Aaltonen Foundation for financial support. KM is funded by the Academy of Finland (336577).

Appendix A. Supplementary data

Supplementary data to this article can be found online at https://doi.org/10.1016/j.renene.2023.119473.

References

[1] IEA, P.V. Solar. https://www.iea.org/reports/solar-pv, 2022. (Accessed 3 October 2022).
[2] D.C. Jordan, Methods for Analysis of Outdoor Performance Data, Presentation, 2011, https://doi.org/10.2172/1009680.
[3] T. Nordmann, L. Clavadetscher, W.G.J.H. van Sark, M. Green, IEA PVPS Task 13 Analysis of Long - Term Performance of PV Systems, Different Data Resolution for Different Purposes, 2014.
[4] D. Atsu, I. Seres, M. Aghaei, I. Farkas, Analysis of long-term performance and reliability of PV modules under tropical climatic conditions in sub-Saharan, Renew. Energy 162 (2020) 285–295, https://doi.org/10.1016/j.renene.2020.08.021.
[5] D. Verma, M. Tayyib, T.O. Saetre, O.M. Midtgard, Outdoor performance of 10 year old a-Si and poly-Si modules in southern Norway conditions, in: 2012 38th IEEE Photovolt. Spec. Conf., IEEE, 2012, pp. 2368–2371, https://doi.org/10.1109/PVSC.2012.6318074.
[6] J. Hedström, L. Palmblad, Performance of Old PV Modules Performance of Old PV Modules—Measurement of 25 Years Old Crystalline Silicone Modules Elforsk, 2006.
[7] S. Lindig, I. Kaaya, K.-A. Weiss, D. Moser, M. Topic, K.A. Weis, D. Moser, M. Topic, Review of statistical and analytical degradation models for photovoltaic modules and systems as well as related improvements, IEEE J. Photovoltaics 8 (2018) 1773–1786, https://doi.org/10.1109/JPHOTOV.2018.2870532.
[8] A. Ameur, A. Berrada, A. Bouaichi, K. Loudiyi, Long-term performance and degradation analysis of different PV modules under temperate climate, Renew. Energy 188 (2022) 37–51, https://doi.org/10.1016/j.renene.2022.02.025.
[9] I. Romero-Fiances, A. Livera, M. Theristis, G. Makrides, J.S. Stein, G. Nofuentes, J. de la Casa, G.E. Georghiou, Impact of duration and missing data on the long-term photovoltaic degradation rate estimation, Renew. Energy 181 (2022) 738–748, https://doi.org/10.1016/j.renene.2021.09.078.
[10] D. Hassan Daher, L. Gaillard, C. Ménézo, Experimental assessment of long-term performance degradation for a PV power plant operating in a desert maritime climate, Renew. Energy 187 (2022) 44–55, https://doi.org/10.1016/j.renene.2022.01.056.
[11] S. Lindig, D. Moser, A.J. Curran, K. Rath, A. Khalilnejad, R.H. French, M. Herz, B. Müller, G. Makrides, G. Georghiou, A. Livera, M. Richter, J. Ascencio-Vásquez, M. van Iseghem, M. Meftah, D. Jordan, C. Deline, W. van Sark, J.S. Stein, M. Theristis, B. Meyers, F. Baumgartner, W. Luo, International collaboration framework for the calculation of performance loss rates: data quality, benchmarks, and trends (towards a uniform methodology), Prog. Photovoltaics Res. Appl. 29 (2021) 573–602, https://doi.org/10.1002/pip.3397.
[12] D.C. Jordan, C. Deline, M.G. Deceglie, A. Nag, G.M. Kimball, A.B. Shinn, J.J. John, A.A. Alnuaimi, A.B.A.A. Elnosh, W. Luo, A. Jain, M.U. Saleh, H. Von Korff, Y. Hu, J.-N.N. Jaubert, F. Mavromatakis, C. Deline, M.G. Deceglie, A. Nag, G.M. Kimball, A.B. Shinn, J.J. John, A.A. Alnuaimi, A.B.A.A. Elnosh, Reducing interanalyst variability in photovoltaic degradation rate assessments, IEEE J. Photovoltaics 10 (2020) 206–212, https://doi.org/10.1109/JPHOTOV.2019.2945191.
[13] A. Phinikarides, G. Makrides, G.E. Georghiou, Comparison of analysis methods for the calculation of degradation rates of different photovoltaic technologies, in: 28th Eur. Photovolt. Sol. Energy Conf, Exhib., 2014, pp. 3973–3976, https://doi.org/10.4229/28thEUPVSEC2013-5BV.4.39.
[14] S. Lindig, A. Louwen, D. Moser, M. Topic, Outdoor PV system monitoring—input data quality, data imputation and filtering approaches, Energies 13 (2020) 5099, https://doi.org/10.3390/en13195099.
[15] A. Livera, M. Theristis, E. Koumpli, S. Theocharides, G. Makrides, J. Sutterlueti, J. S. Stein, G.E. Georghiou, Data processing and quality verification for improved photovoltaic performance and reliability analytics, Prog. Photovoltaics Res. Appl. 29 (2021) 143–158, https://doi.org/10.1002/pip.3349.
[16] D.C. Jordan, S.R. Kurtz, The dark horse of evaluating long-term field performance-data filtering, IEEE J. Photovoltaics 4 (2014) 317–323, https://doi.org/10.1109/JPHOTOV.2013.2282741.
[17] G. Belluardo, P. Ingenhoven, W. Sparber, J. Wagner, P. Weihs, D. Moser, Novel method for the improvement in the evaluation of outdoor performance loss rate in different PV technologies and comparison with two other methods, Sol. Energy 117 (2015) 139–152, https://doi.org/10.1016/j.solener.2015.04.030.
[18] A. Virtuani, D. Strepparava, G. Friesen, A simple approach to model the performance of photovoltaic solar modules in operation, Sol. Energy 120 (2015) 439–449, https://doi.org/10.1016/j.solener.2015.07.045.
[19] B. Kirn, K. Brecl, M. Topic, A new PV module performance model based on separation of diffuse and direct light, Sol. Energy 113 (2015) 212–220, https://doi.org/10.1016/j.solener.2014.12.029.
[20] A. Phinikarides, G. Makrides, N. Kindyni, G.E. Georghiou, Comparison of trend extraction methods for calculating performance loss rates of different photovoltaic technologies, in: 2014 IEEE 40th Photovolt. Spec. Conf., IEEE, 2014, pp. 3211–3215, https://doi.org/10.1109/PVSC.2014.6925619.
[21] P. Ingenhoven, G. Belluardo, D. Moser, Comparison of statistical and deterministic smoothing methods to reduce the uncertainty of performance loss rate estimates, IEEE J. Photovoltaics 8 (2018) 224–232, https://doi.org/10.1109/JPHOTOV.2017.2762523.
[22] D.C. Jordan, M.G. Deceglie, S.R. Kurtz, PV degradation methodology comparison - a basis for a standard, in: 2016 IEEE 43rd Photovolt. Spec. Conf., IEEE, United States, 2016, pp. 273–278, https://doi.org/10.1109/PVSC.2016.7749593.
[23] A. Phinikarides, G. Makrides, B. Zinsser, M. Schubert, G.E. Georghiou, Analysis of photovoltaic system performance time series: seasonality and performance loss, Renew. Energy 77 (2015) 51–63, https://doi.org/10.1016/j.renene.2014.11.091.
[24] S. Lindig, M. Theristis, D. Moser, Best practices for photovoltaic performance loss rate calculations, Prog. Energy. 4 (2022), 022003, https://doi.org/10.1088/2516-1083/ac655f.
[25] A.J. Curran, C. Birk Jones, S. Lindig, J. Stein, D. Moser, R.H. French, Performance loss rate consistency and uncertainty across multiple methods and filtering criteria, in: 2019 IEEE 46th Photovolt. Spec. Conf., 2019, pp. 1328–1334, https://doi.org/10.1109/PVSC40753.2019.8980928.
[26] R.H. French, L.S. Bruckman, D. Moser, S. Lindig, M. von Iseghem, B. Müller, J. S. Stein, M. Richter, M. Herz, W. van Sark, F. Baumgartner, IEA PVPS T13-22:2021: Assessment of Performance Loss Rate of PV Power Systems, 2021. www.iea-pvps.org.
[27] M.G. Deceglie, A. Nag, A. Shinn, G. Kimball, D. Ruth, D. Jordan, J. Yan, K. Anderson, K. Perry, M. Mikofski, M. Muller, W. Vining, C. Deline, NREL/rdtools: Version 2.1.3, https://doi.org/10.5281/zenodo.5826282, 2022.
[28] A. Curran, T. Burleyson, W. Oltjen, S. Lindig, D. Moser, R. French, PVplr: performance loss rate analysis pipeline. https://cran.r-project.org/package=PVplr, 2022.
[29] A.J. Curran, T.L. Burleyson, K. Rath, A.S. Xin, S. Lindig, D. Moser, J. Stein, L. S. Bruckman, R.H. French, PVplr: R package implementation of multiple filters and algorithms for time-series performance loss rate analysis, in: 2020 47th IEEE Photovolt. Spec. Conf., 2020, pp. 2086–2090, https://doi.org/10.1109/PVSC45281.2020.9300807.
[30] S. Lindig, J. Ascencio-Vasquez, J. Leloux, D. Moser, A. Reinders, Performance analysis and degradation of a large fleet of PV systems, IEEE J. Photovoltaics 11 (2021) 1312–1318, https://doi.org/10.1109/JPHOTOV.2021.3093049.
[31] I. Kaaya, S. Lindig, K.A. Weiss, A. Virtuani, M. Sidrach de Cardona Ortin, D. Moser, Photovoltaic lifetime forecast model based on degradation patterns, Prog. Photovoltaics Res. Appl. 28 (2020) 979–992, https://doi.org/10.1002/pip.3280.
[32] B.R. Paudyal, A. Gerd Imenes, Performance assessment of field deployed multi-crystalline PV modules in Nordic conditions, in: 2019 IEEE 46th Photovolt. Spec. Conf., IEEE, 2019, pp. 1377–1383, https://doi.org/10.1109/PVSC40753.2019.8980629.
[33] M.B. Øgaard, H.N. Riise, H. Haug, S. Sartori, J.H. Selj, Photovoltaic system monitoring for high latitude locations, Sol. Energy 207 (2020) 1045–1054, https://doi.org/10.1016/j.solener.2020.07.043.
[34] A. Poskela, L. Karttunen, H. Palonen, H. Huerta, S. Ranta, K. Miettunen, Data processing for photovoltaic performance loss analysis in nordic climate, in: 8th World Conf. Photovolt., Energy Convers., 2022, pp. 666–669, https://doi.org/10.4229/WCPEC-82022-3BV.3.17.
[35] G. Mannino, G.M. Tina, M. Cacciato, L. Todaro, F. Bizzarri, A. Canino, A photovoltaic degradation evaluation method applied to bifacial modules, Sol. Energy 251 (2023) 39–50, https://doi.org/10.1016/j.solener.2022.12.048.
[36] A. Kosonen, J. Ahola, C. Breyer, A. Albo, Large scale solar power plant in Nordic conditions, in: 2014 16th Eur. Conf. Power Electron. Appl., 2014, pp. 1–10, https://doi.org/10.1109/EPE.2014.6911030.
[37] T. Haukkala, Does the sun shine in the High North? Vested interests as a barrier to solar energy deployment in Finland, Energy Res. Social Sci. 6 (2015) 50–58, https://doi.org/10.1016/j.erss.2014.11.005.
[38] M. Formolli, G. Lobaccaro, J. Kanters, Solar energy in the nordic built environment: challenges, opportunities and barriers, Energies 14 (2021) 8410, https://doi.org/10.3390/en14248410.
[39] S. Jouttijärvi, G. Lobaccaro, A. Kamppinen, K. Miettunen, Benefits of bifacial solar cells combined with low voltage power grids at high latitudes, Renew. Sustain. Energy Rev. 161 (2022), 112354, https://doi.org/10.1016/j.rser.2022.112354.
[40] S. Ranta, J.S. Stein, H. Huerta, A. Heinonen, E. Whitney, Self-consumption rate achieved by the bifacial East-West vertical PV system compared to the conventional South facing system in Nordic conditions, in: 36th Eur. Photovolt.

Sol. Energy Conf, Exhib., 2019, pp. 1702–1705, https://doi.org/10.4229/EUPVSEC20192019-6CO.15.5.
[41] S. Guo, T.M. Walsh, M. Peters, Vertically mounted bifacial photovoltaic modules: a global analysis, Energy 61 (2013) 447–454, https://doi.org/10.1016/j.energy.2013.08.040.
[42] Prism solar, bifacial module model Bi60-362/368/375BSTC. www.prismsolar.com. (Accessed 12 September 2023).
[43] ISO 9060:2018, Solar Energy — Specification and Classification of Instruments for Measuring Hemispherical Solar and Direct Solar Radiation, 2018.
[44] S. Bhaduri, A. Kottantharayil, Mitigation of soiling by vertical mounting of bifacial modules, IEEE J. Photovoltaics 9 (2019) 240–244, https://doi.org/10.1109/JPHOTOV.2018.2872555.
[45] Data Portal – New Energy Research Center Turku. https://nerc.turkuamk.fi/data-portal/. (Accessed 16 October 2023).
[46] W. Gu, T. Ma, S. Ahmed, Y. Zhang, J. Peng, A comprehensive review and outlook of bifacial photovoltaic (bPV) technology, Energy Convers. Manag. 223 (2020), 113283, https://doi.org/10.1016/j.enconman.2020.113283.
[47] D.L. King, W.E. Boyson, J.A. Kratochvil, Photovoltaic array performance model. https://doi.org/10.2172/919131, 2004.
[48] W. Gu, T. Ma, S. Ahmed, Y. Zhang, J. Peng, A comprehensive review and outlook of bifacial photovoltaic (bPV) technology, Energy Convers. Manag. 223 (2020), 113283, https://doi.org/10.1016/j.enconman.2020.113283.
[49] E. Mouhib, L. Micheli, F.M. Almonacid, E.F. Fernández, E. Mouhib, L. Micheli, F. M. Almonacid, E.F. Fernández, Overview of the fundamentals and applications of bifacial photovoltaic technology: agrivoltaics and aquavoltaics, Energies 15 (2022) 8777, https://doi.org/10.3390/EN15238777.
[50] IEC 61724-3, Photovoltaic System Performance - Part 3: Energy Evaluation Method, 2016.
[51] W.F. Holmgren, C.W. Hansen, M.A. Mikofski, Pvlib python: a python package for modeling solar energy systems, J. Open Source Softw. 3 (2018) 884, https://doi.org/10.21105/joss.00884.
[52] B. Haurwitz, Insolation in relation to cloudiness and cloud density, J. Meteorol. 2 (1945) 154–166, https://doi.org/10.1175/1520-0469(1945)002<0154:IIRTCA>2.0.CO;2.
[53] B. Haurwitz, Insolation in relation to cloud type, J. Meteorol. 5 (1948) 110–113, https://doi.org/10.1175/1520-0469(1948)005<0110:IIRTCT>2.0.CO;2.
[54] A. Louwen, A.C. de Waal, R.E.I. Schropp, A.P.C. Faaij, W.G.J.H.M. van Sark, Comprehensive characterisation and analysis of PV module performance under real operating conditions, Prog. Photovoltaics Res. Appl. 25 (2017) 218–232, https://doi.org/10.1002/pip.2848.
[55] C. Deline, S. Macalpine, B. Marion, F. Toor, A. Asgharzadeh, J.S. Stein, Assessment of bifacial photovoltaic module power rating methodologies-inside and out, IEEE J. Photovoltaics 7 (2017) 575–580, https://doi.org/10.1109/JPHOTOV.2017.2650565.
[56] J.S. Stein, C. Reise, J.B. Castro, G. Friesen, G. Maugeri, E. Urrejola, S. Ranta, IEA PVPS Task 13 Performance, Operation and Reliability of Photovoltaic Systems - Bifacial Photovoltaic Modules and Systems: Experience and Results from International Research and Pilot Applications, 2021.
[57] IEC 61724-1, Photovoltaic System Performance – Part 1, 2021. Monitoring.
[58] A.P. Dobos, PVWatts version 5 manual. https://doi.org/10.2172/1158421, 2014.
[59] C.M. Whitaker, T.U. Townsend, J.D. Newmiller, D.L. King, W.E. Boyson, J. A. Kratochvil, D.E. Collier, D.E. Osborn, Application and validation of a new PV performance characterization method, in: Conf. Rec. 26th IEEE Photovolt. Spec. Conf., 1997, pp. 1253–1256, https://doi.org/10.1109/pvsc.1997.654315.
[60] T. Huld, G. Friesen, A. Skoczek, R.P. Kenny, T. Sample, M. Field, E.D. Dunlop, A power-rating model for crystalline silicon PV modules, Sol. Energy Mater. Sol. Cells 95 (2011) 3359–3369, https://doi.org/10.1016/j.solmat.2011.07.026.
[61] F. Mavromatakis, F. Vignola, B. Marion, Low irradiance losses of photovoltaic modules, Sol. Energy 157 (2017) 496–506, https://doi.org/10.1016/j.solener.2017.08.062.
[62] P.J. Huber, Robust estimation of a location parameter, Ann. Math. Stat. 35 (1964) 73–101, https://doi.org/10.1214/aoms/1177703732.
[63] E. Hasselbrink, M. Anderson, Z. Defreitas, M. Mikofski, Y.C. Shen, S. Caldwell, A. Terao, D. Kavulak, Z. Campeau, D. Degraaff, Yu-Chen Shen, S. Caldwell, A. Terao, D. Kavulak, Z. Campeau, D. Degraaff, Validation of the PVLife model using 3 million module-years of live site data, in: 2013 IEEE 39th Photovolt. Spec. Conf., IEEE, 2013, pp. 7–12, https://doi.org/10.1109/PVSC.2013.6744087.
[64] PVUSA Project Team, 1989-1990 PVUSA Progress Report, 1990.
[65] C.M. Whitaker, T.U. Townsend, H.J. Wenger, A. Iliceto, G. Chimento, F. Paletta, Effects of irradiance and other factors on PV temperature coefficients, in: Conf. Rec. 22nd IEEE Photovolt. Spec. Conf., 1991, pp. 608–613, https://doi.org/10.1109/pvsc.1991.169283.
[66] D. Micheli, S. Alessandrini, R. Radu, I. Casula, Analysis of the outdoor performance and efficiency of two grid connected photovoltaic systems in northern Italy, Energy Convers. Manag. 80 (2014) 436–445, https://doi.org/10.1016/j.enconman.2014.01.053.
[67] A. Padilla, C. Londoño, F. Jaramillo, I. Tovar, J.B. Cano, E. Velilla, Photovoltaic performance assess by correcting the I-V curves in outdoor tests, Sol. Energy 237 (2022) 11–18, https://doi.org/10.1016/j.solener.2022.03.064.
[68] D.L. King, J.A. Kratochvil, W.E. Boyson, Temperature coefficients for PV modules and arrays: measurement methods, difficulties, and results, in: Conf. Rec. 26th IEEE Photovolt. Spec. Conf., 1997, pp. 1183–1186, https://doi.org/10.1109/pvsc.1997.654300.
[69] B.R. Paudyal, A.G. Imenes, Investigation of temperature coefficients of PV modules through field measured data, Sol. Energy 224 (2021) 425–439, https://doi.org/10.1016/j.solener.2021.06.013.
[70] F. Perin Gasparin, F. Detzel Kipper, F. Schuck de Oliveira, A. Krenzinger, Assessment on the variation of temperature coefficients of photovoltaic modules with solar irradiance, Sol. Energy 244 (2022) 126–133, https://doi.org/10.1016/j.solener.2022.08.052.
[71] S.K. Kwak, J.H. Kim, Statistical data preparation: management of missing values and outliers, Korean J. Anesthesiol. 70 (2017) 407–411, https://doi.org/10.4097/kjae.2017.70.4.407.
[72] S.V. Muravyov, I.A. Marinushkina, Processing data from interlaboratory comparisons by the method of preference aggregation, Meas. Tech. 58 (2016) 1285–1291, https://doi.org/10.1007/s11018-016-0886-4.
[73] P. Barde, M. Barde, What to use to express the variability of data: standard deviation or standard error of mean? Perspect. Clin. Res. 3 (2012) 113–116, https://doi.org/10.4103/2229-3485.100662.
[74] D.C. Jordan, S.R. Kurtz, K. VanSant, J. Newmiller, Compendium of photovoltaic degradation rates, Prog. Photovoltaics Res. Appl. 24 (2016) 978–989, https://doi.org/10.1002/pip.2744.
[75] W. Luo, P. Hacke, K. Terwilliger, Y. Wang, G. Armin, Elucidating potential - induced degradation in bifacial PERC silicon photovoltaic modules, Prog. Photovoltaics Res. Appl. (2018) 859–867, https://doi.org/10.1002/pip.3028.
[76] J. Carolus, J.A. Tsanakas, A. Van Der Heide, E. Voroshazi, W. De Ceuninck, M. Daenen, Physics of potential-induced degradation in bifacial p -PERC solar cells, Sol. Energy Mater. Sol. Cells 200 (2019), 109950, https://doi.org/10.1016/j.solmat.2019.109950.
[77] D.C. Jordan, T.J. Silverman, B. Sekulic, S.R. Kurtz, PV degradation curves: non-linearities and failure modes, Prog. Photovoltaics Res. Appl. 25 (2017) 583–591, https://doi.org/10.1002/pip.2835.
[78] K. Sporleder, V. Naumann, J. Bauer, S. Richter, A. Hähnel, S. Großer, M. Turek, C. Hagendorf, Root cause analysis on corrosive potential-induced degradation effects at the rear side of bifacial silicon PERC solar cells, Sol. Energy Mater. Sol. Cells 201 (2019), 110062, https://doi.org/10.1016/j.solmat.2019.110062.